Applied Soft Computing 13 (2013) 3178–3189

Contents lists available at SciVerse ScienceDirect

Applied Soft Computing

journal homepage: www.elsevier.com/locate/asoc

Quality time-of-flight range imaging for feature-based registration using bacterial foraging

E. Bermejo [a,*], O. Cordón [a,b,c], S. Damas [b], J. Santamaría [d]

[a] Department of Computer Science and Artificial Intelligence, University of Granada, Spain
[b] European Centre for Soft Computing, Mieres, Spain
[c] Centro de Investigación en Tecnologías de La Información y de las Comunicaciones (CITIC-UGR), University of Granada, Spain
[d] Department of Computer Science, University of Jaén, Spain

ARTICLE INFO

Article history:
Received 1 January 2012
Received in revised form 6 July 2012
Accepted 20 August 2012
Available online 1 September 2012

Keywords:
Image registration
Evolutionary computation
3D modelling
Time of flight
Bacterial foraging

ABSTRACT

Image registration is a widely tackled research topic in the computer vision and the computer graphics fields. This problem aims to find an optimal transformation or correspondence between images acquired under different conditions. Recently, a new 3D image acquisition device based on the time-of-flight technology has appeared which obtains range images from real-time 3D video sequences. In this contribution, we aim to study the feasibility of using this new class of cameras to face the 3D model reconstruction procedure. Our proposal is two-fold. First, we introduce a novel image preprocessing pipeline in order to improve the quality of time-of-flight range images and a subsequent feature extraction method considering both 2D and 3D images. As second major objective, we propose an adaptation of the evolutionary bacterial foraging optimization algorithm, which has recently emerged as a very powerful technique for real parameter optimization and gained a high interest for distributed optimization and control, to tackle the range image registration problem. Finally, we analyse the performance of our proposal against other state-of-the-art evolutionary image registration methods.

1. Introduction

In the last decade, 3D range imaging has been widely used in the community in order to obtain 3D models of real-world objects. In the last few years, range imaging-based technology has opened new lines of research in the computer vision (CV) and the computer graphics (CG) fields [1], mainly focused on the processing of the geometry and the topology of range images, e.g. in noise reduction, analysis, segmentation, classification and 3D model reconstruction. 3D representation of real-world scenarios is essential for a wide variety of applications as robotics, automotive engineering, video surveillance or medical imaging [2–4].

One of the greatest challenges of modern range imaging devices has been the acquisition of quality 3D images in real time. Recently, the time-of-flight (ToF) technology used in some real-time 3D video devices, e.g. the Photonic Mixer Device (PMD) [5], has evolved significantly. Unlike traditional range scanners, the image accuracy of this novel technology is highly dependent on resolution and other ambient and light scene factors. As first approach to face these shortcomings, it is necessary to balance the frame rate in order to reduce the source of error. Nevertheless, more suitable solutions are needed to obtain quality 3D images.

Image registration (IR) [6,7] is a fundamental task in CV that aims at finding the optimal transformation between two (or more) images. Such transformation estimation is formulated as an optimization problem where the degree of resemblance between images is measured by a similarity metric. The optimization process applied by traditional IR methods, e.g. the iterative closest point (ICP) algorithm [8,9] is highly influenced by image noise, image discretization, image misalignment, among others. On the other hand, evolutionary computation (EC) [10,11], in particular evolutionary algorithms (EAs) [4,12] have demonstrated its ability to overcome some of the shortcomings of traditional IR methods, achieving a robust performance in complex optimization problems.

Recently, natural swarm inspired algorithms like particle swarm optimization (PSO), ant colony optimization (ACO) have found their way into this domain and proved their effectiveness. Following the same trend of swarm-based algorithms, Passino proposed the BFOA in [13]. Application of group foraging strategy of a swarm of *Escherichia coli* bacteria in multi-optimal function optimization is the key idea of the new algorithm. Bacteria search for nutrients in a manner to maximize energy obtained per unit time. Individual bacterium also communicates with others by sending signals. A bacterium takes foraging decisions after considering two

* Corresponding author.
E-mail addresses: enric2186@correo.ugr.es, enric2186@gmail.com (E. Bermejo), ocordon@decsai.ugr.es (O. Cordón), sergio.damas@softcomputing.es (S. Damas), jslopez@ujaen.es (J. Santamaría).

1568-4946/$ – see front matter © 2012 Elsevier B.V. All rights reserved.
http://dx.doi.org/10.1016/j.asoc.2012.08.041

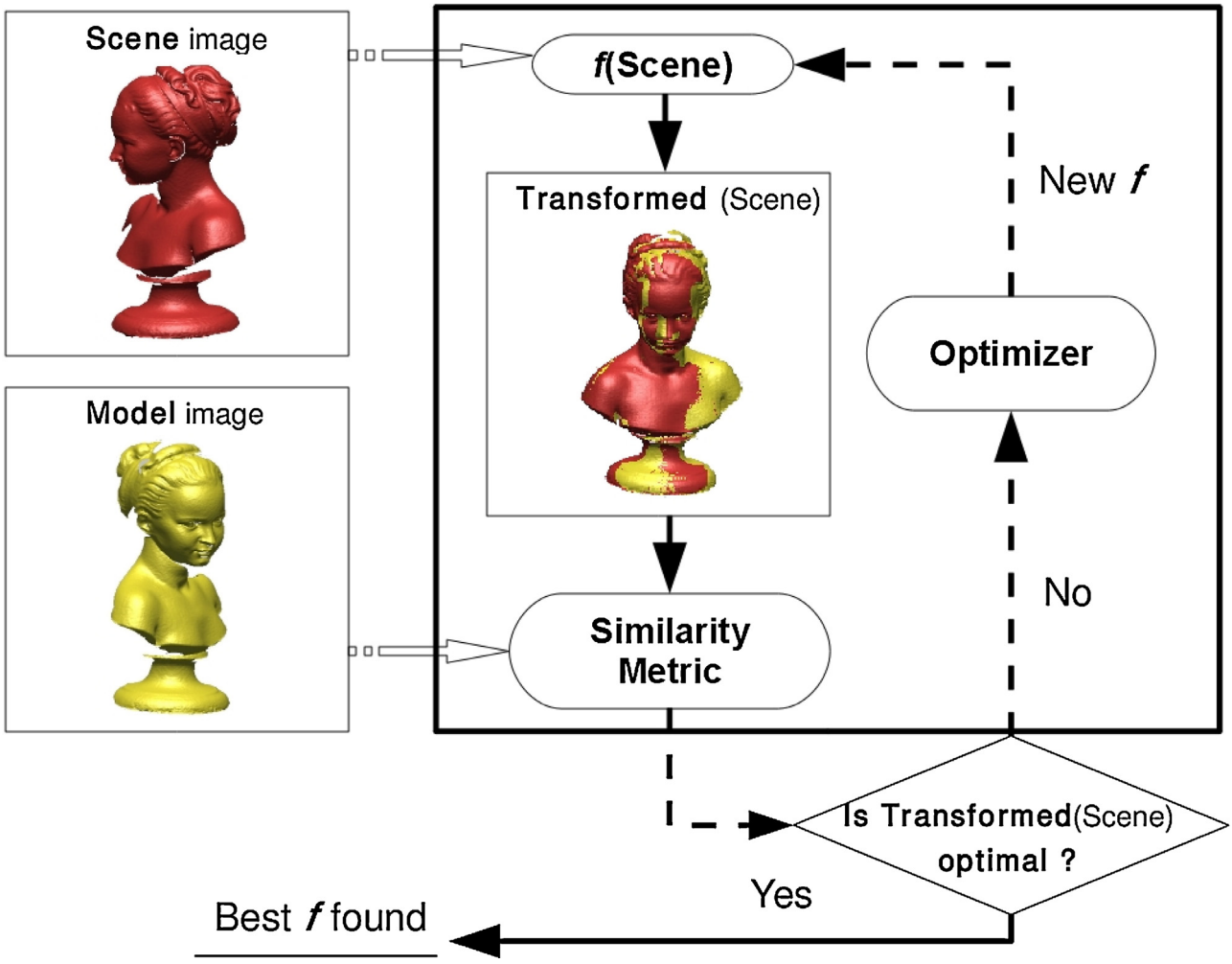

Fig. 1. A general framework of the IR optimization process.

previous factors. The process, in which a bacterium moves by taking small steps while searching for nutrients, is called chemotaxis and key idea of BFOA is mimicking chemotactic movement of virtual bacteria in the problem search space. It has already drawn the attention of researchers because of its efficiency in solving real-world optimization problems arising in several application domains. Unlike others evolutionary-based approaches, the underlying biology behind the foraging strategy of *E. coli* is emulated in an extraordinary manner and used as a simple optimization algorithm. In this work we aim to analyse the performance of a novel design of BFOA facing a challenging real-world problem.

This contribution is structured as follows. Section 2 is aimed to introduce the 3D reconstruction problem using evolutionary computation (EC). Also, this section details the main features of ToF cameras. Next, Section 3 describes our IR proposal based on a specific image processing pipeline using ToF devices and a hybrid EA to tackle the IR problem. Section 4 introduces the experimental study. Finally, Section 5 draws some conclusions and future lines.

2. Background

2.1. Image registration

In the last few years, specialized communities have experienced a growing interest using range scanners for building high-quality 3D models of real-world objects and scenes [14,3], and avoiding humans to manually produce these models using laborious and error-prone CAD-based approaches [15]. To do so, improved techniques within the 3D model reconstruction pipeline, e.g. IR algorithms, has been contributed to date [2].

There is not a universal design for a hypothetical IR method that could be applicable to all registration tasks, since various considerations on the particular application must be taken into account [6]. However, IR methods usually require the following four components (see Fig. 1): two input **Images** named as Scene $I_s = \{\vec{p}_1, \vec{p}_2, \ldots, \vec{p}_n\}$ and Model $I_m = \{\vec{p}_1{}', \vec{p}_2{}', \ldots, \vec{p}_m{}'\}$, with $\vec{p}_i$ and $\vec{p}_j{}'$ being image points; a **Registration transformation** f, being a parametric function relating the two images; a **Similarity metric function** F, in order to measure a qualitative value of closeness or degree of fitting between the transformed scene image, noted $f'(I_s)$, and the model image; and an **Optimizer** that looks for the optimal transformation f inside the defined solution search space.

Usually, the iterative closest point (ICP) algorithm [8,16] is the de-facto standard for doing pair-wise IR of range images to build the 3D models in a process called 3D modelling/reconstruction. However, the success of convergence of the algorithm will depend on the initial pose of the images.[1]

[1] The experiments conducted in [12] demonstrated the poor performance of ICP when facing IR problems considering different degrees of image misalignment.

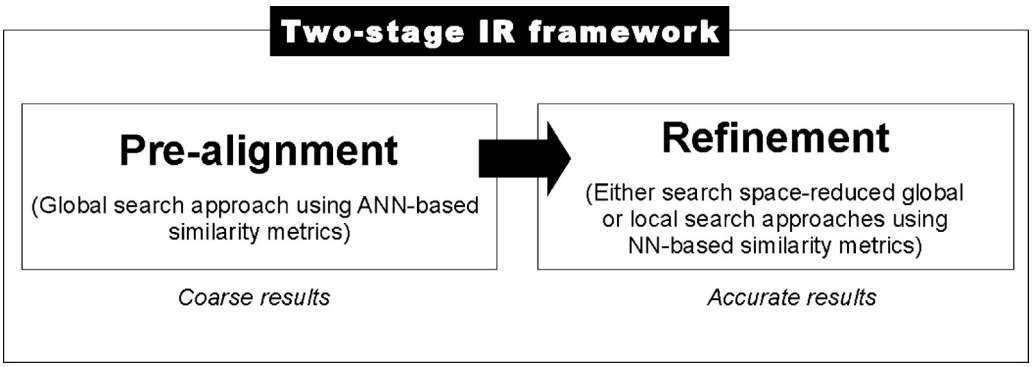

Fig. 2. Pair-wise evolutionary IR approach.

2.2. Evolutionary image registration

As stated before, the Optimizer component is of great importance in the success of the IR procedure. Since the ICP algorithm was introduced, many contributions have been proposed extending and partially solving its shortcomings [17,18,9]. Nevertheless, they still assume it is provided an initial near-optimal alignment of images.

On the other hand, EAs [11,10] make use of computational models of evolutionary processes as key elements in the design and implementation of computer-based problem solving systems. In the last decade, there is an increasing interest on applying EC principles to complex optimization tasks due to their capability to scape from local optima. Genetic algorithms (GAs) [19,20] are the more extensively adopted EAs facing optimization problems. These algorithms are based on the mechanism of natural selection, where the search space of the problem is represented as a collection of individuals (problem solutions) or chromosomes (conforming a population), each of them simultaneously operating on several points of the search space. At every generation (iteration), some of the candidate solutions are paired and parts of each individual (block of genes) are mixed (crossover operator) to form two new solutions, and additionally, every individual is subject to random changes (mutation operator). The next generation is produced by selecting (selection operator) individuals from the current one on the basis of their fitness or *objective function*, which measures how good is each candidate solution and guides the search space exploration strategy. The objective function is one of the most important components of heuristic methods whose design dramatically affects the performance of the method implemented. Optimization procedures using stochastic schemes as those based on EAs are theoretically and empirically found to provide global near-optimal solutions for complex optimization problems, with several of them from the computer vision and the computer graphics fields [21–25].

The first attempts to face the IR problem using EC can be found in the 1980s [26], where a GA [27] was developed for tackling rigid IR of 2D angiography images. Since then, evolutionary IR has become a very active area due to the successful results and several well-known EAs have been considered to tackle the IR optimization process [12].

Unlike ICP-based algorithms, there is no formal proof to asses that EC-based IR methods converge to the global optimum. In order to address this theoretical shortcoming, a two-stage IR approach (see Fig. 2) is usually considered in which a first coarser and time consuming stage using EAs, named as pre-alignment, and a refinement step usually[2] applying ICP-based IR algorithms are applied in a serialized fashion. Despite this limitation, evolutionary IR methods are able to achieve accurate results even without requiring any refinement stage as we will see in Section 4.

2.3. Time of flight cameras

ToF cameras are able to capture real-time 3D video. In particular, PMD scanners are based on the time-of-flight principle. Usually, they consist on a CCD or a CMOS sensor and some LEDs or laser diodes that illuminate the scene with a continuous modulated light, which is reflected by the object surface and demodulated in the receiver. The difference between the emitted light and the reflected one generates a phase delay which is used to measure the distances:

$$D_i = \frac{c\varphi_i}{4\pi f_{mod}} \quad (1)$$

where f_{mod} is the modulated signal frequency, c is the light speed, and φ_i is the phase shift of the signal.

Additionally, the phase delay generates an offset from which it is possible to obtain more information about the signal, e.g. intensity or amplitude values. Specifically, the PMD scanner has a 204×204 resolution, 25 fps frame rate, and a CMOS sensor with suppression of background illumination (SBI) features which allows to measure distances between 0.3 and 7 m. However, one of the main limitations of the real-time 3D video devices is their low resolution [29–32], reaching values between 62×32 and 640×860 pixels. Other difficulties are the appearance of systematic errors as the generation of perfect sinusoidal modulated signal (distance-related error) or by the non-linearity of the electronic components (amplitude-related error). Moreover, non-systematic measurement errors occur when ToF cameras illuminate the whole scene at once. Usually, pixels have a high dynamic range generated by the reflectivity of the object itself, thus leading to measurement errors mostly motivated by cross-reflections or inter-reflections when the signal is reflected on several surfaces (corners, concave objects, etc.).

3. Image registration proposal

This section is devoted to introduce both the novel image preprocessing pipeline including feature extraction and the hybrid evolutionary IR algorithm proposed to tackle problem instances considering range images acquired by ToF devices.

3.1. Image processing pipeline

As said, it is necessary to reduce the source of noise in order to improve the quality of range images acquired by ToF cameras. Our novel approach uses a three-staged pipeline scheme in which range images obtained from 3D video sequences are enhanced by

[2] Other refinement approaches have been utilized [28].

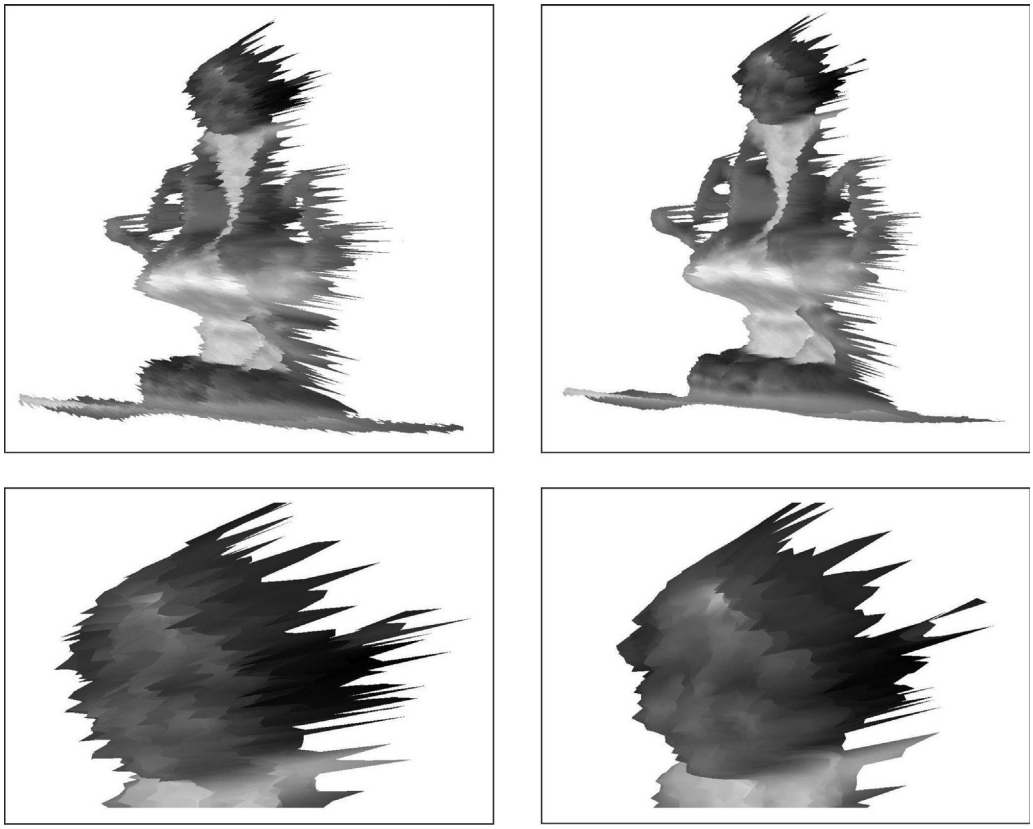

Fig. 3. Comparison between the original acquired image (left column) and the corresponding image when the first stage is applied (right column).

successively reducing the level of noise. Next, the improved images are used to obtain a small set of robust 3D features (that will guide the IR process) as final step of the procedure. The first stage faces the noise introduced in the calibration of the emitted signal [33] and consists on the acquisition of an averaged image of the object by means of considering different values of both the integration time and the modulated frequency parameters. Additionally, the frame rate is reduced, which is a quite effective solution as can be shown in Fig. 3.

Despite the application of this first noise reduction stage, distance measurements are not accurate enough. Median or amplitude correction filters can be used [34]. Nevertheless, these solutions are prone to provide robust results in presence of remaining noise. Then, the second stage uses an enhancement technique based on the *Shading Constraint* [35] principle. This technique follows the *Shape from Shading* (SfS) [36] approach which is based on the statistical dependence between range (3D) and intensity (2D) information. The code of this stage was provided by the *Action Recognition and Tracking based on Time-of-Flight Sensors* project (ARTTS, http://www.artts.eu). Fig. 4 shows enhanced results using this novel technique when considering the local albedo operation mode [35].

Quality improvement of range images achieved following these stages is decisive for the subsequent third stage, i.e. 3D feature extraction. This last step of the proposed pipeline aims to obtain a reduced subset of characteristic range image points in order to both speed up and guide the optimization process of the subsequent IR task. Specifically, it allows to extract two subsets of 3D features as follows:

- First, the method proposed by Castellani et al. [37] is used to extract a small quantity of disperse interest points. This technique builds a geometric descriptor for every salient point which allows to derive information about prominence levels, curvature, and normals. The main advantage of this method is its robustness against noise, holes and occlusions.
- The previous subset of features is increased with additional points taking advantage of the intensity (gray-level) value acquired for each range image point. To do so, we considered the *Speeded Up Robust Features* (SURF) [38] algorithm which is one of the most used invariant feature extraction methods in CV due to its robustness against to noise, errors, and geometric distortions.

Then, our feature extraction proposal exploits the 2D intensity values to extract more relevant information, thus avoiding certain problems shown by similar methods when corrupted 3D geometric information is present. Fig. 5 shows a graphical summary of the proposed image preprocessing pipeline.

3.2. Hybrid bacterial foraging algorithm

Recently, Passino has proposed the BFOA search strategy [13] has proposed the BFOA search strategy [13]. It is based on the *foraging* approach of the *E. coli* bacteria, which consists on the following four steps:

3.2.1. Chemotaxis

This process simulates the foraging behaviour of the bacteria according to movement in two different ways. Depending on the food concentration, it swims for a period of time in the same direction or it tumbles to change its current direction. Mathematically, $\theta^i(j, k, l)$ represents the ith bacterium in the jth chemotactic, kth

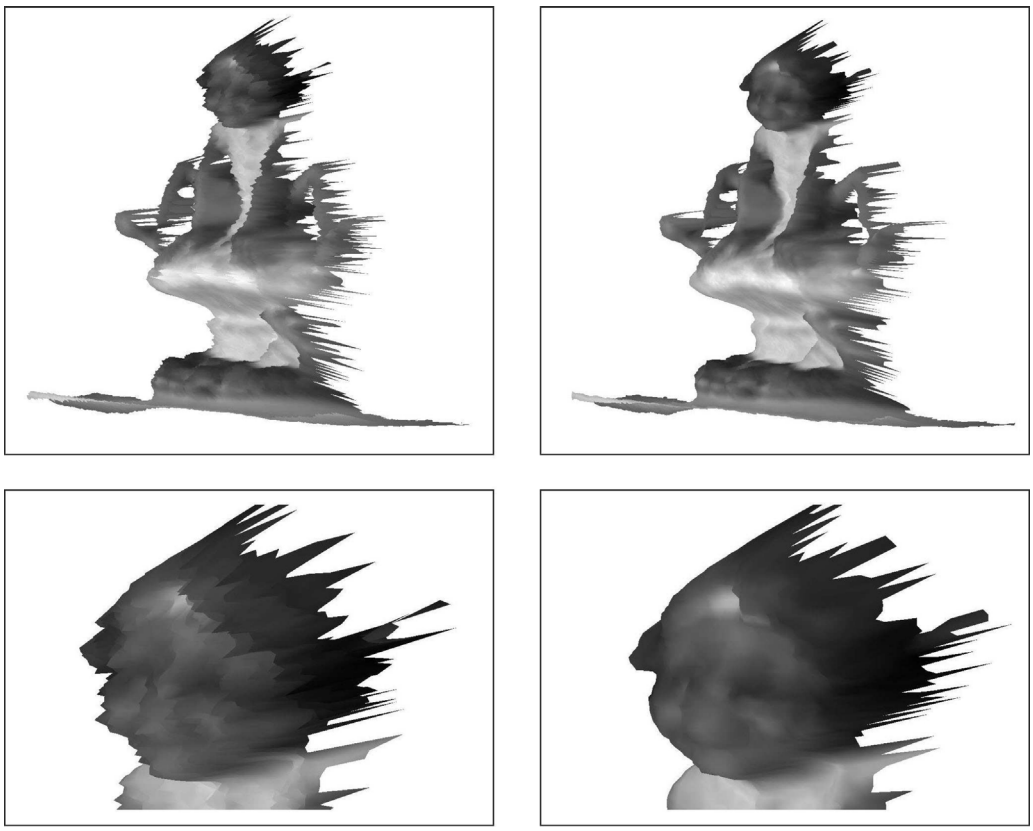

Fig. 4. Comparison between the image obtained in the first stage (left column) and the subsequent one provided in the second stage (right column).

reproductive, and *l*th elimination and dispersal phases. The tumble movement is modelled as in [13]:

$$\phi(i) = \frac{\Delta(i)}{\sqrt{\Delta(i)^T \Delta(i)}} \tag{2}$$

where Δ indicates a random vector which direction lies in the range $[-1, 1]$. Thus, the chemotactic step is defined:

$$\theta^i(j+1, k, l) = \theta^i(j, k, l) + C(i)\phi(i) \tag{3}$$

where $C(i)$ represents the step size taken during the swim step.

3.2.2. Swarming

A social behaviour is simulated in this stage. Those bacteria placed in locations with high amount of nutrients tends to attract other bacteria, while those placed in hazardous zones tend to repel them. This cell to cell attraction-repulsion behaviour is modelled as follows:

$$J_{cc}(\theta, P(j, k, l)) = \sum_{i=1}^{S} J_{cc}(\theta, \theta^i(j, k, l))$$

$$= \sum_{i=1}^{S} [-d_{attract}\, exp(-w_{attract} \Sigma_{m=1}^{p} (\theta_m - \theta_m^i)^2)]$$

$$+ \sum_{i=1}^{S} [-h_{repell}\, exp(-w_{repell} \Sigma_{m=1}^{p} (\theta_m - \theta_m^i)^2)] \tag{4}$$

where $J_{cc}(\theta, P(j, k, l))$ is the swarming value to be added to the objective function during the chemotactic step j; S is the total number of bacteria; p is the number of variables (or dimensionality of the problem) to be optimized; $d_{attract}$, $w_{attract}$, h_{repell}, and w_{repell} are different coefficients that represent the attractant and the repellant intensity factors of the bacteria.

3.2.3. Reproduction

The least healthy bacteria, i.e. those who have found less amount of nutrients during the chemotaxis, will die during the reproductive step. On the other hand, the most healthy bacteria will be asexually split in two bacteria. Only the first half of the bacteria will be considered for reproduction by means of replacing the remaining bacteria in order to keep the swarm size constant.

3.2.4. Elimination-dispersal

The last step consists on the elimination or dispersal of some bacteria based on the simulation of sudden or gradual changes in the local environment, e.g. a rise of the temperature may kill a group of bacteria within a region. This event is simulated by the elimination of some bacteria with a small probability and randomly initializing a new bacteria for replacement.

The pseudo-code of the canonical BFOA [13] is described in the following:

Step 1 Initialize p, S, N_c, N_s, N_{re}, N_{ed}, P_{ed}, $C(i)$, θ^i
where:
p: search space dimension
S: total number of bacterium in the population
N_c: number of chemotaxis steps
N_s: maximum number of swims
N_{re}: number of reproductive steps
N_{ed}: number of elimination-dispersal steps

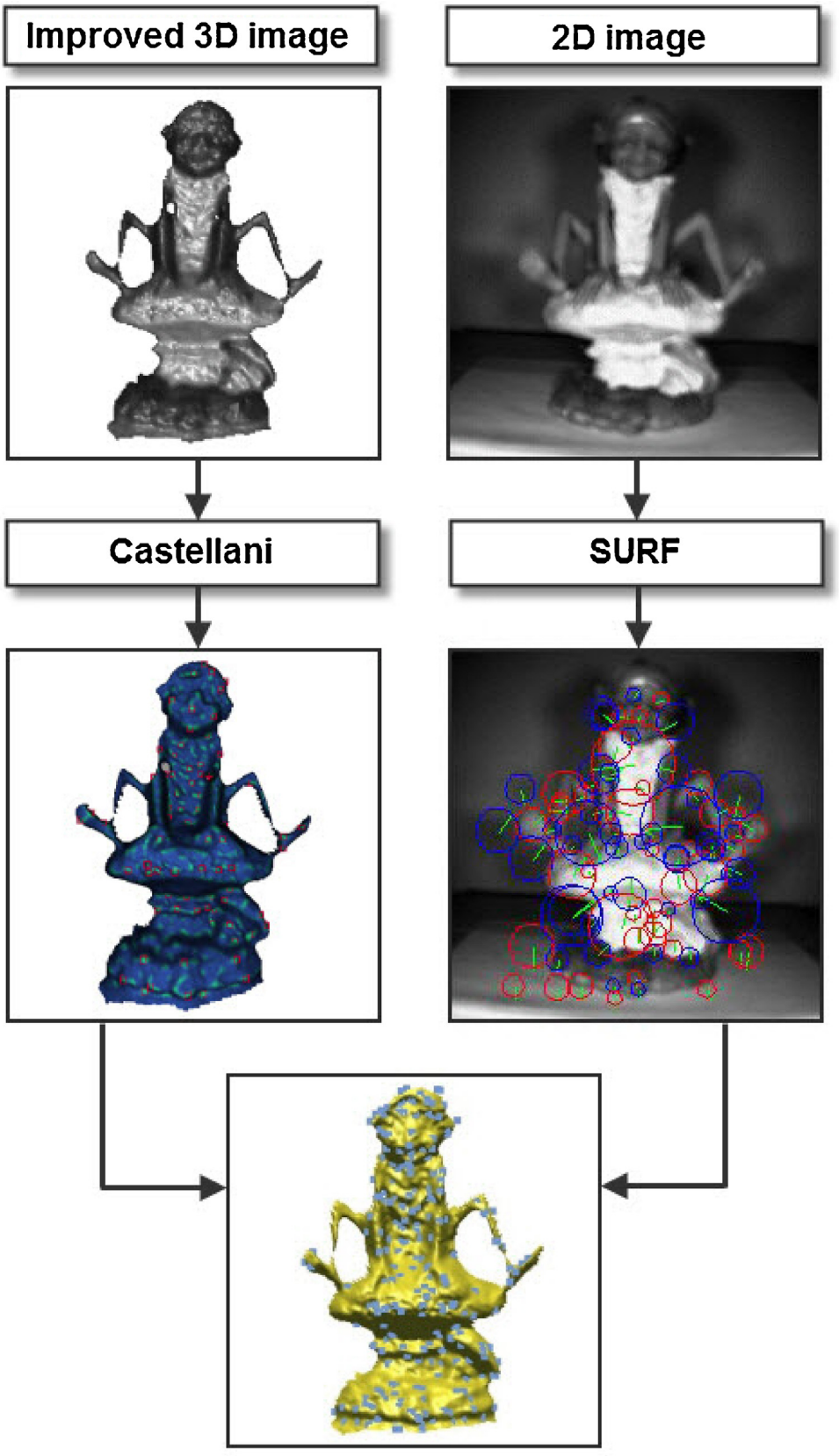

Fig. 5. The proposed image preprocessing pipeline.

P_{ed}: elimination-dispersal probability
$C(i)$: chemotaxis step size
θ^i: bacterium i

Step 2 Elimination-dispersal loop $l = l + 1$:
Step 3 Reproduction loop $k = k + 1$:
Step 4 Chemotaxis loop $j = j + 1$:
For $i = 1, \ldots, S$ take the chemotactic step:
(a) Compute fitness:
$J(i, j, k, l) = J(i, j, k, l) + J_{cc}(\theta^i(j, k, l), P(j, k, l))$
(b) Tumble:
(i) Generate a random vector: $\Delta_m(i)$, $m = 1, \ldots, p$
(ii) Move: $\theta^i(j+1, k, l) = \theta^i(j, k, l) + C(i)(\Delta(i)/\sqrt{\Delta(i)^T\Delta(i)})$
(iii) Compute the new fitness value $J(i, j+1, k, l)$
(c) Swim:
Initialize $m = 0$; While $m < N_s$ Do
- $m = m + 1$
- If $J(i, j, k, l) < J_{last}$
update J_{last}
move: $\theta^i(j+1, k, l) = \theta^i(j, k, l) + C(i)(\Delta(i)/\sqrt{\Delta(i)^T\Delta(i)})$
- Else
$m = N_s$. This is the end of the while statement and the chemotactic step for bacterium i

(d) Repeat the process with the next bacterium $i = i + 1$ while $i \neq S$
Step 5 If $j < N_c$ go to Step 4
Step 6 Reproduction:
(a) For each bacterium, k and l, compute:

$$J^i_{health} = \sum_{j=1}^{N_c+1} J(i, j, k, l) \tag{5}$$

to represent the total health of the bacterium i along its lifetime. Sort bacteria in ascending order of J_{health}
(b) The worst S_r bacteria (those with the highest J_{health} values) are replaced with the copies of those bacteria with lower J_{health} values
Step 7 If $k < N_{re}$ go to Step 3
Step 8 Elimination-Dispersal: eliminate the entire pool of bacteria with probability P_{ed}
Step 9 If $l < N_{ed}$ go to Step 2
Otherwise End

The main shortcoming of the canonical BFOA is the oscillation of the state of the bacteria when they are close to the optimal values, performing a considerable number of unnecessary chemotactic steps. In order to avoid this, Dasgupta et al. [39] proposed a refined variant in which the step size is adapted as follows:

$$C = \frac{|J(\theta)|}{|J(\theta)| + \lambda} = \frac{1}{1 + \lambda/|J(\theta)|} \tag{6}$$

where λ is a positive constant. Thus, when $J(\theta)$ is large the step size is accordingly increased ($C \to 1$), and it will be decreased once the bacteria approaches the global optima. This adaptive approach outperforms the canonical BFOA as shown in [39]. Our hybrid BFOA (HBFOA) proposal is based on the latter. Additionally, HBFOA incorporates the following novel components to achieve a more suitable performance tackling the IR problem:

- It may occur in the original reproduction step that the bacterium with less accumulated life (J_{health}) is not the best bacterium in the swarm. We propose an alternative based on a probabilistic selection of the best bacteria. Instead of sorting the bacteria in ascending order of their accumulated J_{health} values, a probabilistic filter is applied previous to sorting of the bacteria. In first place, the current life value of each bacteria is normalized considering the life accumulated during the chemotaxis. Then, the best fit bacteria to be reproduced are selected with inverse probability of this normalized value. Finally, the bacteria are sorted and the first half reproduce as in the original method. This strategy increases the importance of those bacteria that obtain best fitness values in the last chemotactic cycles.
- Despite the elimination-dispersal step considers a small probability of application (1/8), we tested the performance of the algorithm usually gets down, thus losing the progress achieved in the chemotactic steps. Thus, we have considered the best bacterium found so far to guide the dispersal step in order to minimize the negative impact of killing the best bacterium. Moreover, each transformation parameter has a 30% probability of being similar to the best bacterium.
- Besides, we introduce a set of elite solutions with the M (5) best solutions found. After each chemotactic step, if the algorithm finds a solution, p_{new}, better than the worst elite solution, e_m, a recombination mechanism is applied considering p_{new} and a randomly selected elite solution. Recombination is done by using the *BLX-α* operator [40]. In case of the new solution, r_{new}, is better than p_{new}, the former will replace both the worst elite solution, e_m, and its parent. Otherwise, p_{new} will replace both e_m and its parent.
- Finally, we have introduced a local search (LS) strategy as a hybridization with the Dasgupta et al.'s BFOA variant. In particular, we considered the crossover-based LS (XLS) [41] method which has obtained promising results in previous works [42]. XLS is applied after the reproduction step.

3.3. Coding scheme and objective function

As said, the 3D model reconstruction pipeline involves the application of several pair-wise alignments of two adjacent range images (see Fig. 1) in order to obtain the final 3D model of the physical object [3]. Therefore, every pair-wise IR method aims to find the Euclidean motion that brings the *scene* view (I_s) into the best possible alignment with the *model* view (I_m). An Euclidean motion is usually considered based on a 3D rigid transformation (f) determined by six or seven real-coded parameters when using either Euler or axis plus angle representation for rotation, respectively. Specifically, Euler-based rotation matrices suffer from the pitfall of the *gimbal-lock* and specialized literature recommends using the second scheme. Thus, we define the rigid transformation as: a rotation $R = (\theta, Axis_x, Axis_y, Axis_z)$ and a translation $\vec{t} = (t_x, t_y, t_z)$, with θ and $\vec{Axis}$ being the angle and axis of rotation, respectively. Then, the transformed points of the *scene* view are denoted by

$$f(\vec{p}_i) = R(\vec{p}_i) + \vec{t}, \qquad i = \{1, \ldots, n\} \tag{7}$$

where n is the number of points of the I_s image. Hence, the pair-wise RIR procedure based on EAs can be formulated as an optimization problem developed to search for the Euclidean transformation[3] f^* achieving the best alignment of both $f(I_s)$ and I_m

$$f^* = \arg\min_f F(I_s, I_m; f) \quad s.t.: \quad f^*(I_s) \cong I_m \tag{8}$$

according to the Similarity metric, F, being optimized. Among others, the median square error (MedSE) is usually considered as the F function in 3D modelling [43] due to its robustness in presence of outliers (e.g. acquired noisy range images) are present in the RIR process, and it can be formulated as:

[3] For optimization, any RIR solution is represented as a seven-dimensional real-coded vector $x = \langle \theta, Axis_x, Axis_y, Axis_z, t_x, t_y, t_z \rangle$.

Table 1
Number of feature points extracted once the third step of the proposed pipeline is applied.

	Goblin		*Teddy*		*Pirate*	
	0°	45°	0°	45°	0°	45°
Raw	11,468	10,983	13,802	13,641	11,340	10,210
Features	224	228	261	259	254	224

Table 2
Parameter settings used in Passino, Dasgupta, and HBFOA algorithms.

Parameter	Value	Description
n_p	7	Problem dimension.
n_s	16	Swarm size.
N_c	30	Number of chemotactic steps.
N_s	20	Number of swims.
N_{re}	6	Number of reproductive steps.
$Prob_{ed}$	0.125	Elimination-dispersal probability.
N_{ed}	3	Number of elimination-dispersal steps.
C_i	0.1	Step length (fixed only for Passino).
λ	0.0001	Constant value used to calculate the step length (C_i) in Dasgupta and HBFOA algorithms.

$$F(I_s, I_m; f) = MedSE(d_i^2), \quad \forall i = \{1, \ldots, n\} \tag{9}$$

where $MedSE()$ corresponds to the median value of all the squared Euclidean distances, d_i^2, between the transformed scene point, $f(\vec{p}_i)$, and its corresponding closest point, $\vec{p}'_j$, in the *model* view I_m, that is:

$$d_i^2 = \|f(\vec{p}_i) - \vec{p}'_j\|^2, \quad j = \{1, \ldots, m\} \tag{10}$$

where m is the number of points of the I_m image. Notice that, it can be said that both the F function and either the fitness or the objective function (see Section 2.2) have the same meaning within the optimization process. In order to speed up the computation of the closest point of every $f(\vec{p}_i)$ point, indexing structures as kd-trees [28] or the grid closest point (GCP) transform [44] are often used. Specifically, we have considered the kd-tree scheme together with a random sampling of the cloud points in our later experimental study.

4. Experiments

4.1. Datasets

The range images used in the experiments were obtained from video sequences acquired using a PMD[Vision]® Camcube 2.0 camera considering three different objects. Each scan has been carried out every 45 rotation degrees using a turn table [18]. Fig. 6 shows the snapshots of the three considered objects, named: Goblin, Teddy, and Pirate. The left column depicts the obtained range images by using the first two steps of the proposed pipelined image processing scheme (Section 3.1).

Table 1 shows the number of points of both the preprocessed range image (raw data) and the extracted features using the proposed image processing pipeline (Section 3.1). It is remarkable the reduced size of data the IR method should deal with, thereby it will allow to speed up such a procedure.

4.2. Experimental design

Each problem instance to be tackled consists on the registration of two adjacent views (0° and 45°) of every of the three considered objects. We compared the performance of our proposal, HBFOA, against to the Passino's canonical BFOA [13] (Passino) and the Dasgupta et al.'s improved BFOA variant [39] (Dasgupta). Besides, we

Table 3
Statistical results obtained in the prealignment stage for each dataset showing minimum (m), mean (μ) and standard deviation (σ) values of MedSE. Results are scaled ($\times 10^3$).

	Goblin			*Teddy*			*Pirate*		
	m	μ	σ	m	μ	σ	m	μ	σ
Passino	0.00610	0.01211	0.00243	0.01222	0.04671	0.03222	0.00625	0.00853	0.00325
Dasgupta	0.00569	0.01064	0.00383	**0.01182**	0.01594	0.00249	0.00634	**0.00728**	0.00046
HBOFA	**0.00561**	**0.00760**	0.00275	0.01226	**0.01413**	0.00140	0.00647	0.00730	0.00052
ICP-L	0.01167	0.01314	0.00027	0.02788	14.7746	20.8366	0.00746	2.74628	0.50859
GA-C	2.49962	303.279	346.837	11.3260	440.990	498.899	3.29864	412.714	520.820
GA-S	0.00947	0.09527	0.07582	0.01638	0.29109	0.38431	0.00598	0.13806	0.37838
PSO-W	0.00842	0.01208	0.00087	0.01710	0.03689	0.01461	**0.00594**	0.00982	0.00276
SS-S	0.00568	0.00971	0.00340	0.01220	0.01446	0.00161	0.00653	0.00738	0.00039

Bold values highlight the best value obtained for minimum and mean results considering each dataset.

Table 4
Statistical results obtained in the refinement stage for each dataset showing minimum (m), mean (μ) and standard deviation (σ) values of MedSE. Results are scaled ($\times 10^3$).

	Goblin			*Teddy*			*Pirate*		
	m	μ	σ	m	μ	σ	m	μ	σ
Passino	0.00522	0.00896	0.00151	0.01164	0.02181	0.02115	0.00549	0.00581	0.00012
Dasgupta	0.00519	0.00777	0.00224	**0.01163**	0.01205	0.00014	0.00552	0.00577	0.00011
HBFOA	**0.00518**	**0.00611**	0.00179	0.01169	**0.01198**	0.00015	0.00553	**0.00573**	0.00013
ICP-L	0.00934	0.00978	0.00008	0.01215	0.01284	0.00034	0.00579	0.00589	0.00002
GA-C	0.01296	0.07843	0.02832	0.02851	0.46021	0.23071	0.02499	0.07598	0.03782
GA-S	0.00525	0.06017	0.04673	0.01209	0.09637	0.08075	0.00547	0.03242	0.02784
PSO-W	0.00522	0.00942	0.00112	0.01199	0.01295	0.00144	**0.00546**	0.00586	0.00012
SS-S	**0.00518**	0.00700	0.00180	0.01172	0.01202	0.00015	0.00554	0.00577	0.00011

Bold values highlight the best value obtained for minimum and mean results considering each dataset.

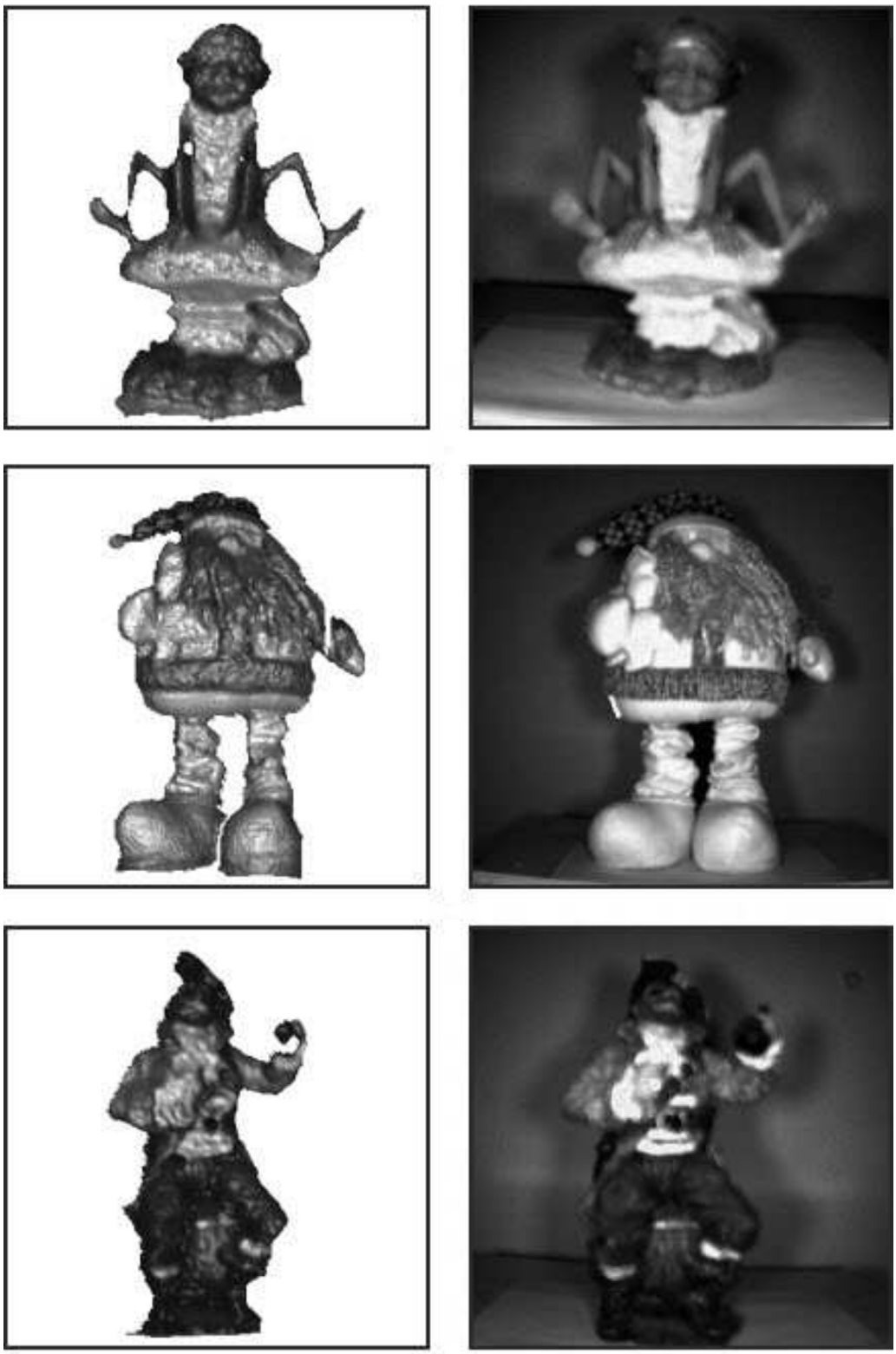

Fig. 6. 3D/2D snapshots of the three objects (*Goblin*, *Teddy*, and *Pirate*) acquired using the PMD camera. Textured range images (left) and their corresponding photo (right) are shown.

considered some of the most relevant state-of-the-art IR evolutionary algorithms:

- Luck et al.'s [45] method, which is based on ICP and annealing (ICP-L).
- Chow et al.'s [46] method. It makes use of GAs (GA-C).
- Silva et al.'s [28] method, which makes use of GAs (GA-S).
- Wachowiak et al.'s [47] method. It is based on the particle swarm optimization (PSO) [48] algorithm (PSO-W).
- Santamaría et al.'s [49] method, which is based on the Scatter Search (SS) [50] algorithm (SS-S).

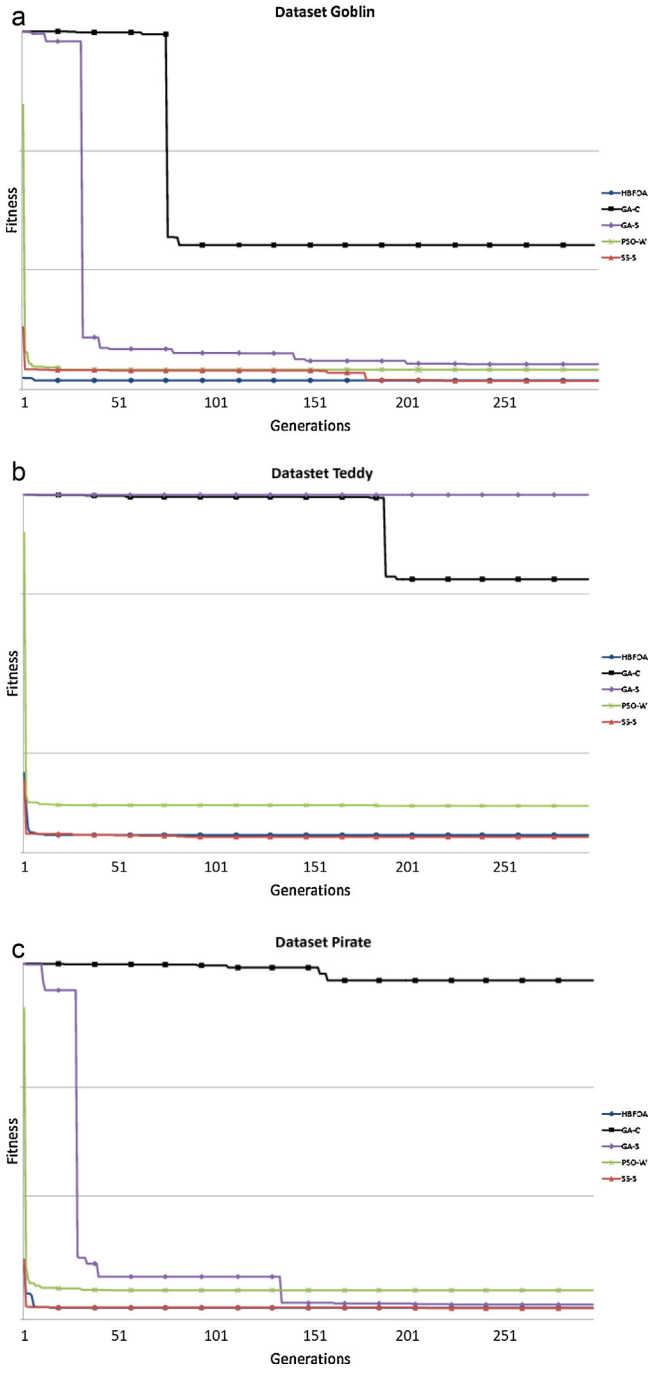

Fig. 7. Convergence study of the tested algorithms facing the Goblin, Teddy, and Pirate datasets.

We considered the CPU time as the stop criterion of the prealignment stage (see Section 2.2) in order to perform a fair comparison of all the IR methods. After a preliminary study, we determined that 20 s is a suitable value once noticed that every method properly converge to accurate enough solutions. In order to avoid execution dependence, 30 different runs of each IR algorithm have been performed in every problem instance. Additionally, we have set 40 iterations for the refinement step which makes use of the ICP-based algorithm [9].

4.3. Parameter settings

All the IR methods were run on an Intel® Core™ i7 2.93 GH platform with 4 GB RAM and implemented using C/C++and the GNU/g++compiler under the GNU/Linux Ubuntu 10 operating system. For every IR algorithm of the literature, we used the parameter values recommended by the authors in their contributions. Table 2 shows the parameter values considered in Passino, Dasgupta, and HBFOA.

4.4. Analysis of results

Tables 3 and 4 show the results of the prealignment and the refinement stages, respectively. These numerical results refer to the mentioned MedSE metric (Eq. (9)) using a Kdtree-based nearest neighbour rule instead of the GCP one considered in the objective function (see Section 3.3).

Regarding the prealignment results, all the BFOA-based IR methods obtain better performance, according to the mean value, than the rest of the methods of the state-of-the-art. Specifically, HBFOA obtains the best mean results in two of the three problem instances (*Goblin* and *Teddy*) and a similar one in the third dataset (*Pirate*) compared with the adaptive BFOA (Dasgupta). According to the minimum values, both HBFOA and Dasgupta IR methods obtain the best results in *Goblin* and *Teddy* instances, respectively. PSO-W achieves the best minimum outcomes in the *Pirate* instance.

Table 4 shows the refinement results. Quite similar outcomes are obtained compared to the prealignment stage, in which HBFOA demonstrates to be the most robust IR method. As shown in [18], all the IR algorithms using the EC paradigm provide accurate enough prealignment solutions that favour the proper convergence of the ICP-based IR method considered for refinement. Specifically, HBFOA obtains the best mean performance in the three problem instances and the best minimum in the *Goblin* dataset. Dasgupta, SS-S, and PSO-W achieve accurate results in the remaining instances.

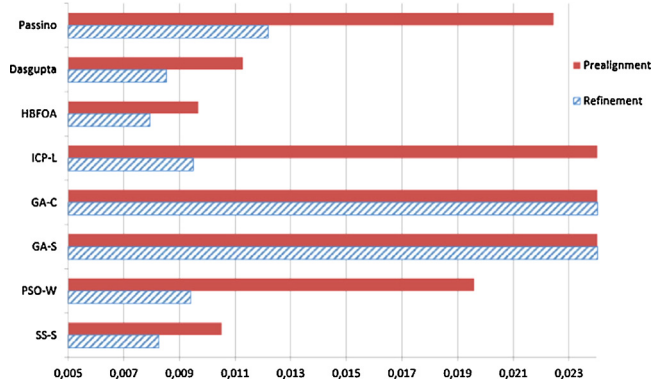

Fig. 8. Averaged performance of all the IR methods in the three considered problem instances when applying the prealignment and the refinement stages. Results are scaled ($\times 10^3$).

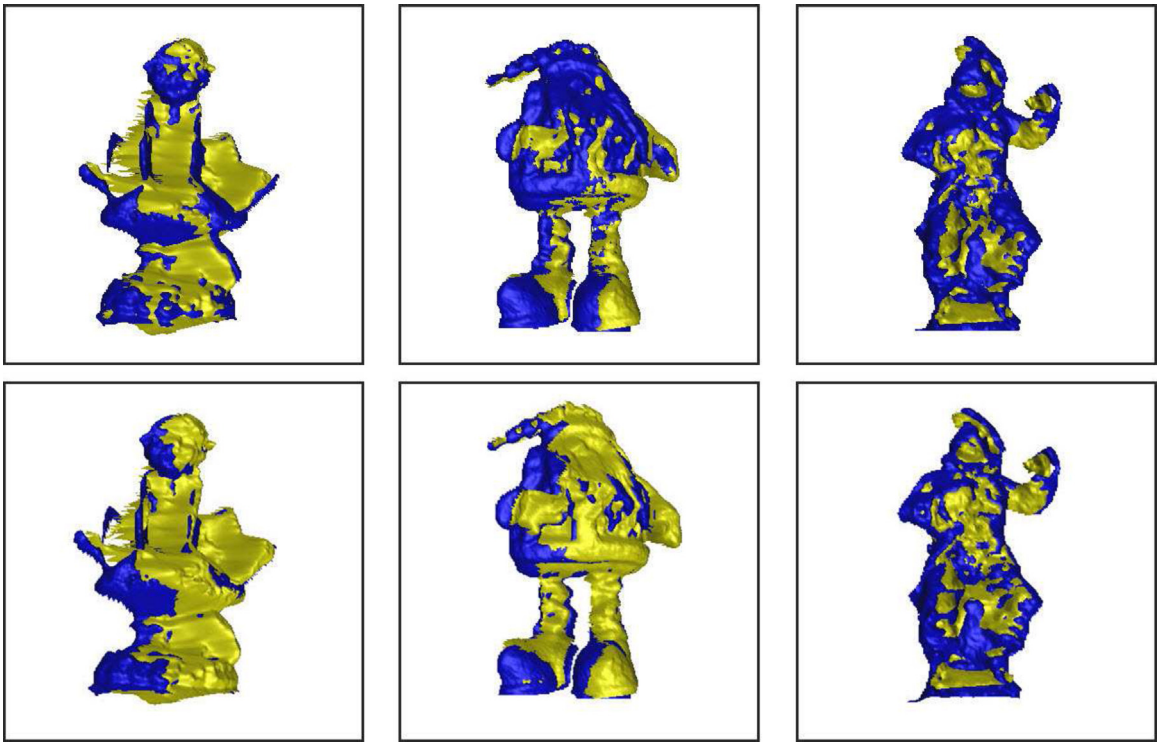

Fig. 9. 3D snapshots of the best IR estimations obtained by our HBFOA proposal for the considered datasets *Goblin*, *Teddy*, and *Pirate* after the prealignment (first row) and the refinement (second row) stages.

These results confirm that our proposal, HBFOA, provides a competitive performance compared to the state-of-the-art IR methods. Fig. 7 shows the convergence velocity of the evolutionary algorithms in the three problem instances. Fig. 8 shows the averaged performance (according to mean value of MedSE) obtained by every algorithm in the three problem instances when applied the prealignment and the refinement stages. This graphic remarks the importance of obtaining an accurate enough prealignment result to promote a suitable convergence of the refinement process. Fig. 9 shows the best prealignment and refinement results obtained by HBFOA in every problem instance.

5. Conclusion and future works

In this work, we have conducted a viability study of using video sequences of ToF cameras to tackle 3D reconstruction problems using evolutionary IR techniques. Our first contribution consists on a novel image preprocessing pipeline which provides an enhanced range image and a subsequent feature extraction procedure. Specifically, we adopted recent advances in both computer vision and computer graphics fields to develop the latter procedure.

The second major contribution refers to the proposal of an improved variant of the bacterial foraging optimization algorithm for tackling the IR problem. Our hybrid evolutionary IR algorithm has proved to be better than previous bacteria foraging approaches and it also obtains a very competitive performance when compared to the most relevant state-of-the-art IR methods. Thus, we have demonstrated the suitability of using the proposed evolutionary approach to address the 3D reconstruction problem.

Due to the increasing interest of recent market in new ToF devices, we expect the emergence of new cameras offering enhanced features. Specifically, the Microsoft Kinect™ is a cutting-edge camera which allows to acquire 3D video images of higher resolution than those obtained by similar scanners such as the PMD. Furthermore, we plan to carry out a comparative study of 3D reconstruction results using different devices based on this recent technology.

Acknowledgements

This work is partially supported by both the Spanish Ministerio de Educación y Ciencia (Ref. TIN2009-07727) including EDRF fundings and the University of Jaén (Ref. R1/12/2010/61) including fundings from *Caja Rural de Jaén*.

References

[1] R.C. González, R.E. Woods, Digital Image Processing, Prentice-Hall, Upper Saddle River, NJ, 2002.
[2] R.J. Campbell, P.J. Flynn, A survey of free-form object representation and recognition techniques, Computer Vision and Image Understanding 81 (2) (2001) 166–210.
[3] F. Bernardini, H. Rushmeier, The 3D model acquisition pipeline, Computer Graphics Forum 21 (2) (2002) 149–172.
[4] S. Damas, O. Cordón, J. Santamaría, Medical image registration using evolutionary computation: a survey, IEEE Computational Intelligence Magazine 6 (4) (2011) 26–42.
[5] Z. Xu, R. Schwarte, H. Heinol, B. Buxbaum, T. Ringbeck, Smart pixel – photonic mixer device (PMD) new system concept of a 3D-imaging camera-on-a-chip, in: 5th Int. Conf. on Mechatronics and Machine Vision in Practice, 1998, pp. 259–264.
[6] B. Zitová, J. Flusser, Image registration methods: a survey, Image and Vision Computing 21 (2003) 977–1000.
[7] J. Salvi, C. Matabosch, D. Fofi, J. Forest, A review of recent range image registration methods with accuracy evaluation, Image and Vision Computing 25 (5) (2007) 578–596.
[8] P.J. Besl, N.D. McKay, A method for registration of 3D shapes, IEEE Transactions on Pattern Analysis and Machine Intelligence 14 (1992) 239–256.
[9] Z. Zhang, Iterative point matching for registration of free-form curves and surfaces, International Journal of Computer Vision 13 (2) (1994) 119–152.
[10] T. Bäck, D.B. Fogel, Z. Michalewicz, Handbook of Evolutionary Computation, IOP Publishing Ltd. and Oxford University Press, New York, EEUU, 1997.
[11] A. Eiben, J. Smith, Introduction to Evolutionary Computation, Springer, Berlin, 2003.
[12] J. Santamaría, O. Cordón, S. Damas, A comparative study of state-of-the-art evolutionary image registration methods for 3D modeling, Computer Vision and Image Understanding 115 (2011) 1340–1354.

[13] K. Passino, Biomimicry of bacterial foraging for distributed optimization and control, IEEE Control Systems Magazine 22 (3) (2002) 52–67.
[14] M. Levoy, K. Pulli, B. Curless, S. Rusinkiewicz, D. Koller, L. Pereira, M. Ginzton, S. Anderson, J. Davis, J. Ginsberg, J. Shade, D. Fulk, The Digital Michelangelo Project: 3D scanning of large statues, in: ACM SIGGRAPH 2000, 2000, pp. 131–144.
[15] G. Dalley, P. Flynn, Range image registration: a software platform and empirical evaluation, in: Third International Conference on 3-D Digital Imaging and Modeling (3DIM'01), 2001, pp. 246–253.
[16] Y. Chen, G. Medioni, Object modelling by registration of multiple range images, Image and Vision Computing 10 (3) (1992) 145–155.
[17] J. Feldmar, N. Ayache, Rigid, affine and locally affine registration of free-form surfaces, International Journal of Computer Vision 18 (2) (1996) 99–119.
[18] Y. Liu, Improving ICP with easy implementation for free form surface matching, Pattern Recognition 37 (2) (2004) 211–226.
[19] D.E. Goldberg, Genetic Algorithms in Search and Optimization, Addison-Wesley, New York, EEUU, 1989.
[20] J.H. Holland, Adaptation in Natural and Artificial Systems, The University of Michigan Press, Ann Arbor, 1975.
[21] Z.H. Hu, Y.S. Ding, W.B. Zhang, Q. Yan, An interactive co-evolutionary CAD system for garment pattern design, Computer-Aided Design 40 (12) (2008) 1094–1104.
[22] W. Pang, K. Hui, Interactive evolutionary 3D fractal modeling, The Visual Computer (2010) 1–17.
[23] X. Qin, Y. Yang, Estimating parameters for procedural texturing by genetic algorithms, Graphical Models 64 (2002) 19–39.
[24] A. Wiens, B. Ross, Gentropy: evolving 2D textures, Computer Graphics 26 (1) (2002) 75–88.
[25] L. Simon, O. Teboul, P. Koutsourakis, N. Paragios, Random exploration of the procedural space for single-view 3D modeling of buildings, International Journal of Computer Vision (2010) 1–19.
[26] J. Fitzpatrick, J. Grefenstette, D. Gucht, Image registration by genetic search, in: IEEE Southeast Conference, Louisville, EEUU, 1984, pp. 460–464.
[27] Z. Michalewicz, Genetic Algorithms + Data Structures = Programs, third ed., Springer-Verlag, Berlin, 1996.
[28] L. Silva, O.R.P. Bellon, K.L. Boyer, Precision range image registration using a robust surface interpenetration measure and enhanced genetic algorithms, IEEE Transactions on Pattern Analysis and Machine Intelligence 27 (5) (2005) 762–776.
[29] R. Lange, 3D time-of-flight distance measurement with custom solid-state image sensors in CMOS/CCD-technology, Ph.D. Thesis, University of Siegen, 2000.
[30] B. Büttgen, T. Oggier, M. Lehmann, R. Kaufmann, F. Lustenberger, CCD/CMOS lock-in pixel for range imaging: challenges, limitations and state-of-the-art, in: 1st Range Imaging Research Day, 2005, pp. 21–32.
[31] S. Fuchs, S. May, Calibration and registration for precise surface reconstruction with ToF cameras, in: Proceedings of the Dynamic 3D Imaging Workshop in Conjunction with DAGM (Dyn3D), vol. 1, Citeseer, 2007.
[32] S. May, 3D Time-of-Flight Ranging for Robotic Perception in Dynamic Environments, Ph.D. Thesis, Universität Osnabrück, 2009.
[33] S. Fuchs, G. Hirzinger, Extrinsic and depth calibration of ToF-cameras, in: 2008 IEEE Conference on Computer Vision and Pattern Recognition, 2008, pp. 1–6.
[34] S. Oprisescu, D. Falie, M. Ciuc, V. Buzuloiu, Measurements with ToE cameras and their necessary corrections, in: 2007 International Symposium on Signals, Circuits and Systems (July), 2007, pp. 1–4.
[35] M. Böhme, M. Haker, T. Martinetz, E. Barth, Shading constraint improves accuracy of time-of-flight measurements, Computer Vision and Image Understanding 114 (12) (2010) 1329–1335.
[36] J.E. Cryer, M. Shah, Shape-from-shading: a survey, IEEE Transactions on Pattern Analysis and Machine Intelligence 21 (8) (1999) 690–706.
[37] U. Castellani, M. Cristani, S. Fantoni, V. Murino, Sparse points matching by combining 3D mesh saliency with statistical descriptors, Computer Graphics Forum 27 (2) (2008) 643–652.
[38] H. Bay, A. Ess, T. Tuytelaars, L. Vangool, Speeded-up robust features (SURF), Computer Vision and Image Understanding 110 (3) (2008) 346–359.
[39] S. Dasgupta, S. Das, A. Abraham, A. Biswas, Adaptive computational chemotaxis in bacterial foraging optimization: an analysis, IEEE Transactions on Evolutionary Computation 13 (4) (2009) 919–941.
[40] L.J. Eshelman, Real-coded genetic algorithms and interval schemata, in: L.D. Whitley (Ed.), Foundations of Genetic Algorithms 2, Morgan Kaufmann, San Mateo, EEUU, 1993, pp. 187–202.
[41] H.G. Beyer, K. Deb, On self-adaptive features in real-parameter evolutionary algorithms, IEEE Transactions on Evolutionary Computation 5 (3) (2001) 250–270.
[42] J. Santamaría, O. Cordón, S. Damas, J. García-Torres, A. Quirin, Performance evaluation of memetic approaches in 3D reconstruction of forensic objects, Soft Computing 13 (8–9) (2009) 883–904.
[43] M. Rodrigues, R. Fisher, Y. Liu, Special issue on registration and fusion of range images, Computer Vision and Image Understanding 87 (1–3) (2002) 1–7.
[44] S.M. Yamany, M.N. Ahmed, A.A. Farag, A new genetic-based technique for matching 3D curves and surfaces, Pattern Recognition 32 (1999) 1817–1820.
[45] J.P. Luck, C.Q. Little, W. Hoff, Registration of range data using a hybrid simulated annealing and iterative closest point algorithm, in: IEEE International Conference on Robotics and Automation (ICRA'00), 2000, pp. 3739–3744.
[46] C.K. Chow, H.T. Tsui, T. Lee, Surface registration using a dynamic genetic algorithm, Pattern Recognition 37 (2004) 105–117.
[47] M.P. Wachowiak, R. Smolikova, Y. Zheng, J.M. Zurada, A.S. El-Maghraby, An approach to multimodal biomedical image registration utilizing particle swarm optimization, IEEE Transactions on Evolutionary Computation 8 (3) (2004) 289–301.
[48] J. Kennedy, R. Eberhart, Particle swarm optimization, in: IEEE International Conference on Neural Networks, vol. 4, 1995, pp. 1942–1948.
[49] J. Santamaría, O. Cordón, S. Damas, I. Alemán, M. Botella, A Scatter Search-based technique for pair-wise 3D range image registration in forensic anthropology, Soft Computing 11 (2007) 819–828.
[50] M. Laguna, R. Martí, Scatter Search: Methodology and Implementations in C, Kluwer Academic Publishers, Boston, 2003.